

PACS numbers: 42.62.Cf; 42.30.Wb; 05.10.Ln
DOI: 10.1070/QE2006v036n02ABEH013120

Monte Carlo simulation of optical clearing of paper in optical coherence tomography

M.Yu. Kirillin, A.V. Priezzhev, J. Hast, R. Myllylä

Abstract. **Signals of an optical coherence tomograph from paper samples are calculated by the Monte Carlo method before and after the action of different immersion liquids such as ethanol, glycerol, benzyl alcohol, and 1-pentanol. It is shown within the framework of the model used that all these liquids reduce the contrast of the inhomogeneity image in upper layers of the samples, considerably improving, however, the visibility of lower layers, allowing the localisation of the rear boundary of a medium being probed, which is important for precision contactless measuring a paper sheet thickness, for example, during the manufacturing process. The results of calculations are in well agreement with experimental data.**

Keywords: *optical coherence tomography, coherence length, light scattering, Monte Carlo simulation, optical clearing of paper, contactless measurements.*

1. Introduction

Optical coherence tomography (OCT) is one of the most promising methods for non-invasive studying the internal structure of optically inhomogeneous objects. In particular, it seems that this method can be used in paper industry for rapid and precision measurements of paper properties during its manufacturing. The methods employed at present such as, for example, electron microscopy and laser confocal microscopy require a long analysis of the data obtained and additional treatment of samples and can considerably change their properties. Therefore, the study of paper by new laser and optical methods being developed at present seems to be quite promising [1].

M.Yu. Kirillin Department of Physics, M.V. Lomonosov Moscow State University, Vorob'evy gory, 119992 Moscow, Russia; Faculty of Technology, Optoelectronics and Measurement Techniques Laboratory, University of Oulu, P.O. Box 4500, 90014 Oulu, Finland; e-mail: mkirillin@yandex.ru, kirillin@ee.oulu.fi;
A.V. Priezzhev Department of Physics, M.V. Lomonosov Moscow State University, Vorob'evy gory, 119992 Moscow, Russia; International Laser Center, M.V. Lomonosov Moscow State University, Vorob'evy gory, 119992 Moscow, Russia; e-mail: avp2@mail.ru;
J. Hast, R. Myllylä Faculty of Technology, Optoelectronics and Measurement Techniques Laboratory, University of Oulu, P.O. Box 4500, 90014 Oulu, Finland;
e-mail: jukka.hast@ee.oulu.fi, risto.myllyla@ee.oulu.fi

Received 3 November 2005; revision received 10 January 2006
Kvantovaya Elektronika **36** (2) 174 – 180 (2006)
Translated by M.N. Sapozhnikov

The OCT method, which was first proposed in 1991 [2] and features a high resolution, rapid scanning, and does not require a long preliminary treatment of samples, can be potentially used to control the paper quality. A coherence tomograph is based on a Michelson interferometer with a sample placed in the object arm and a mirror moving at a constant velocity in the reference arm. The interference of light waves incident on a photodetector from the reference and object arms produces the output signal as a superposition of sets of interference fringes. Each of the sets is a partial interference signal formed due to the superposition of radiation reflected from the reference mirror and radiation reflected by an object (interface or a particle). The envelope of this signal is determined by the coherence function of the light source, while its amplitude depends on the refractive-index mismatch at the interface and on the attenuation of light in the medium.

Therefore, the shorter is the coherence length, the higher is the longitudinal (in the probing direction) resolution of the OCT system. Its resolution with a superluminescent diode (SLD) source is typically 10 μm. The OCT method provides high-quality images of the internal structure of objects weakly scattering light in the visible and near-IR regions. Strongly scattering regions present inside an object under study distort the tomograph signal, which can give incorrect information on the object.

To reduce the scattering order in OCT, clearing liquids (CLs) are used. The clearing effect is achieved when a liquid with the refractive index close to that of the components of a strongly scattering region replaces the substance with a substantially different refractive index in the volume under study, which results in a change in the scattering properties of the region [3].

Scattering and reflection of light occurs at the interface between media with different refractive indices. Refraction from such an interface is described by the Snell law and reflection is determined by the Fresnel coefficients. A scatterer in a medium is a region with the refractive index different from that of the environment. If refractive indices are sufficiently close to each other and the scatterer size is large enough ($n_1/n_2 < 1.05, R \gg \lambda$, optically soft particles), the scattering anisotropy is rather high and the propagation direction of a photon changes insignificantly after scattering. In the opposite case, the scattering effect is quite large, resulting in a considerable change in the propagation direction and a rapid chaotisation of the photon motion, thereby distorting an OCT signal. To avoid these distortions, the refractive-index mismatch of the environment (air, in the case of paper) and scatterers is reduced by introducing

a CL to the environment, which makes the scatterers even more optically soft.

Figure 1 shows the typical structure of a paper sample. Paper consists of wood fibres between which air is found. According to the requirements to the paper quality, fillers of different sizes are added to the paper pulp (initial material) during the manufacturing process, which can also present in the paper sample. The thickness of wood fibres is usually 5 – 20 μm, whereas their length can achieve a few millimetres. These fibres are pressed to layers during paper manufacturing. The typical thickness of paper is equal to the thickness of seven – eight fibres.

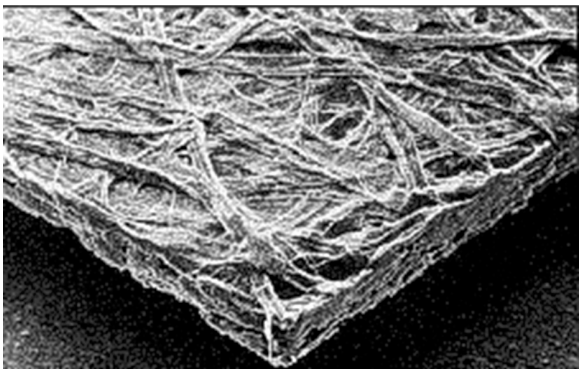

Figure 1. Scanning electron microscope microphotography of a ~ 100-μm thick paper sheet.

One of the urgent problems of paper industry is a contactless high-precision measurement of the paper thickness. This problem can be solved by the OCT method; however, because of a strong light scattering in paper, CLs should be used. In particular, to measure the paper thickness, it is necessary to visualise the rear boundary of a sample, which can be achieved by means of a CL. The CL for a paper sample should have the following properties: (i) its refractive index should be close to that of the wood fibres and fillers; (ii) it should not penetrate into wood fibres, only filling air cavities inside the sample; and (iii) it should not react chemically with fibres and fillers.

In this paper, we consider a multilayer model simulating the internal structure of paper. Note that, to simplify calculations, we studied not individual fibres but continuous layers of fibres, where scattering is characterised by optical parameters known from the literature. To simplify the model, we assume that a sample consists of planar or nonplanar alternating layers with the same optical properties as those of wood fibres and air. The air layers can also contain particles with properties corresponding to those of particles used as paper fillers in paper manufacturing. Depending on the porosity (air content) of a sample being simulated, the thickness of fibre layers was varied from 5 to 18 μm. As a base model, we used in our calculations a nine-layer model containing five fibre layers and four air layers (the total thickness was 100 μm). One of the variants of this model was considered in our previous paper [4].

According to the requirements considered above, we chose several CLs, which are widely used for optical clearing of various objects, including biological tissues [5 – 7]. These liquids have different refractive indices because the optical clearing of paper can be used for two purposes: the visualisation of the internal structure of a sample (layer boundaries in our model) and high-precision measurements of the sample thickness. Based on the values of the refractive index for wood fibres and fillers and also on the requirements presented above, we chose ethanol (the refractive index is 1.36), 1-pentanol (1.41), glycerol (1.47), and benzyl alcohol (1.54) as CLs.

We assumed in simulations that CLs do not penetrate into fibre layers but completely fill all the air cavities between them. In addition, the optical clearing of paper samples with these CLs was studied experimentally [8]. Although it was shown in [8] that some of the liquids are inconvenient to use due to their rapid evaporation or long penetration time into a sample, we consider all them for the generality of model experiments because our main goal is to analyse the influence of a decrease in the refractive-index mismatch on the scattering properties of paper. The aim of this paper is to determine the efficiency of the above-mentioned CLs for optical clearing of paper for obtaining its OCT images.

2. Monte Carlo simulation of the OCT signal

The Monte Carlo method is based on the calculation of many random photon trajectories in a scattering medium, whose optical properties determine the length and shape of individual trajectories, and on the subsequent statistical processing of the results obtained. The main input parameters of simulations are the scattering and absorption coefficients μ_s and μ_a, the anisotropy factor g, and the refractive index n.

The model signal of a tomograph is calculated by using the distribution of photons, contributing to the signal, over their free paths in a medium [9 – 12]. Then, the interference signal is calculated from the expression

$$I(t) = \sum_{\Delta l} [I_r I_s(t, \Delta l)]^{1/2} \cos\left(\frac{2\pi}{\lambda}\Delta l\right) \exp\left[-\left(\frac{\Delta l}{l_{coh}}\right)^2\right], \qquad (1)$$

where I_r and I_s are the intensities of radiation from the reference and object arms, respectively; Δl is the optical path difference; and I_{coh} is the coherence length of the SLD. The exponential factor in expression (1) gives the Gaussian shape of the coherence function of the radiation source. The coherence length was set equal to 15 μm in accordance with the parameters of the real OCT system [13].

To increase the efficiency of the Monte Carlo method, we used the scheme of the so-called implicit accounting for absorption, according to which not one photon but a group or a packet of photons, characterised by some weight, propagates along each random path [14]. This approach allows one to take into account comparatively simply absorption and repeated reflection at the interfaces of the medium and to reduce considerably the calculation time by preserving its accuracy. One OCT signal upon scanning inside a sample (A scan) was calculated by using five million photon packets. The interference signal was calculated by assuming that each photon packet interferes independently with radiation from the reference arm.

As mentioned above, the OCT signal from an object is a superposition of interference patterns determined by inhomogeneities of the optical properties inside the object. By calculating this signal from a multilayer sample simulating

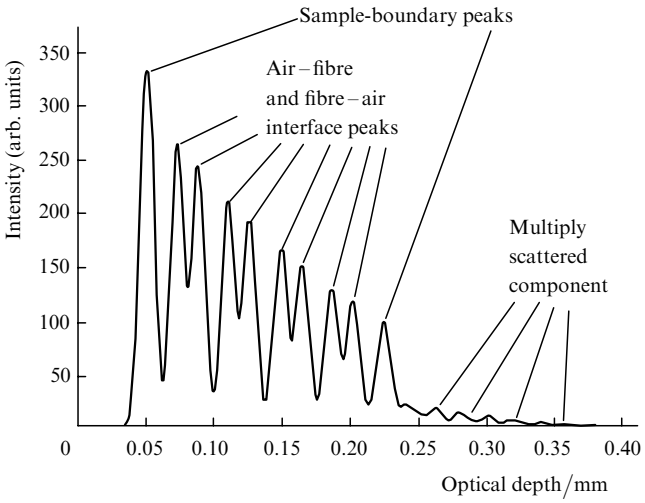

Figure 2. Typical envelope of the OCT signal from a model nine-layer paper sample.

paper, we obtain a set of interference signals from the boundaries of layers because they are the main reflecting regions in the sample. These signals can be overlapped if the distance between the reflecting interfaces does not exceed the coherence length of the source.

Figure 2 presents the typical envelope of the model OCT signal from an 'idealised' paper sample consisting of nine planar layers. The signal exhibits distinct peaks caused by ten boundaries of the layers. The low-intensity peaks following after the tenth peak (which corresponds to the rear boundary of the sample) are caused by multiple scattering of light in paper.

3. Description of the model

We have failed to find the values of scattering and absorption coefficients for wood fibres in the available literature and estimated them from the parameters obtained in [15] by using the Kubelka – Munk theory assuming that the average density of fibres is 80 g m^{-2}. Based also on the data presented in [15 – 17], we used in simulations the values $\mu_s = 16$ mm^{-1}, $\mu_a = 0.5$ mm^{-1}, $g = 0.94$, and $n = 1.53$. Filler particles were simulated by spherical particles with radii from 0.1 to 1.0 μm and the refractive index $n = 1.53$ [16], which were present in the air layers of model samples. We assumed that paper samples have the multilayer structure. To estimate the influence of the paper porosity on the clearing effect, this characteristic was varied from 20 % to 80 %.

Note also that the structure and optical properties of the medium exclude the possibility of solving the problem of radiation propagation in paper analytically, i.e., of solving the main equation of the radiation transfer theory. The numerical solution of this equation will be extremely time-consuming because of the complex boundary conditions. At the same time, simplified theories such as the Kubelka – Munk theory or diffusion theory neglect the specific features of the paper structure and consider it as a homogeneous medium, which is inapplicable for studying the visualisation of the internal structure of paper. All this makes the Monte Carlo method used in this paper most suitable for solving this problem.

The literature known to the authors does not contain information on the phase function of wood fibres, however, their anisotropy factor $g = 0.94$ is presented in [16]. Because a change in the propagation direction of a photon in a sample is mainly caused by its interaction with the layer boundaries rather than with particles, and only forward scattering is important upon scattering inside the layer, we described scattering in fibres with the help of the Heyney – Greenstein phase function

$$f_{HG}(\theta) = \frac{1}{4\pi}\frac{1-g^2}{(1+g^2-2g\cos\theta)^{3/2}}, \qquad (2)$$

which is often used to describe anisotropic scattering. The phase function for spherical filler particles was calculated by using the Mie theory. The phase functions for fillers were calculated separately for each CLs because they depend on the refractive index of the CL. The parameters of the OCT setup used in simulations correspond to the those of the real OCT system described in our paper [8], where OCT signals were also simulated by the Monte Carlo method.

4. Results and discussion

4.1 Paper samples with planar layers

Model OCT signals from a nine-layer sample of thickness 100 μm were calculated for different values of the porosity assuming that layers were planar. The fibre layer thickness was varied from 4 to 16 μm to change the porosity, while the total thickness of a sample remained constant. The addition of a CL to the sample was simulated by varying the refractive index of the air layer by the value of the refractive index of the given CL. The typical set of envelopes of the OCT signal from a sample with a porosity of 40 % obtained for different CLs is presented in Fig. 3. Each peak in this figure corresponds to the air – fibre or fibre – air interface. The first and last peaks correspond to the sample boundaries, while peaks between them correspond to the internal boundaries of the layers and give information on the internal structure of the sample. The lower-intensity peaks located behind the rear-boundary peak are produced by photons multiply reflected from layer boundaries.

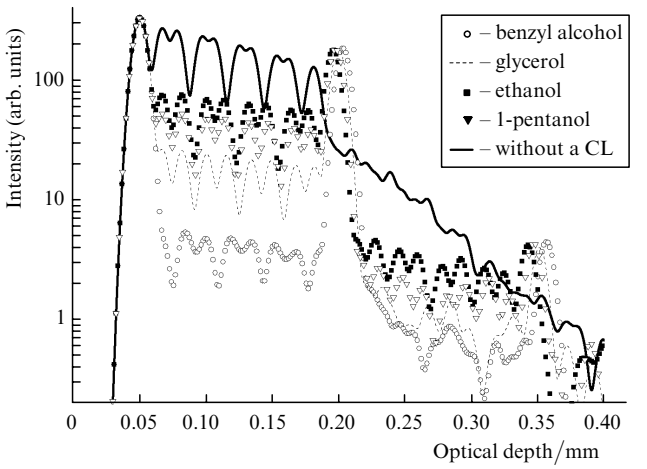

Figure 3. Model OCT signals from a paper sample with the 40 % porosity obtained by using different CLs.

One can see from Fig. 3 that the intensity of the rear-boundary peak increases after the addition of a CL. At the same time, the intensities of peaks corresponding to the internal boundaries of layers decrease with decreasing the refractive-index mismatch of the fibre and CL. Therefore, to visualise the rear boundary in the best way, it is necessary to use CLs with the refractive index close to that of fibres (glycerol or benzyl alcohol). However, in this case the visualisation of the internal structure of the sample can be inadequate. The use of CLs with lower refractive indices provides a better visualisation of the internal layer boundaries. The presence of peaks on the decaying diffusion 'tail' (at the optical depth ~ 0.35 mm) when CLs are used is explained by multiple reflections of photons from the external boundaries of the sample and a weaker scattering inside the sample due to optical clearing.

The visualisation of the internal structure of a paper sample by means of a CL strongly depends on the sample structure. The lower is the paper porosity, the stronger is scattering in fibres and the greater is the contribution of multiple scattering to the signal, resulting in the image distortions. The high porosity reduces scattering in fibres and makes paper more transparent; as a result, the quality of its visualisation by means of OCT improves. We characterised quantitatively the visualisation of the internal structure of paper in this model by the intensity of the peak corresponding to the fourth interlayer boundary. Note also that the partial signals from the adjacent boundaries of layers can overlap if the distance between the boundaries is smaller than the coherence length of a superluminescent diode, which is manifested in their higher intensities compared to the intensity of a signal from one interface. Figure 4 presents the dependences of the intensities of the fourth peak and the rear-boundary peak on the paper porosity obtained by using different CLs. In the case of the 50 % porosity, the thickness of the fibre and air layers is approximately the same, which is manifested in a weak overlap of adjacent peaks and in a decrease in the fourth-peak intensity. One can see from Fig. 4 that the addition of CLs leads to a considerable increase in the rear-boundary peak intensity, decreasing, however, the intensity of peaks corresponding to the internal boundaries of layers, which affects the visualisation of the internal structure of the sample.

Our model neglects the speckle-modulation of the OCT signal caused by the interference of photon packets for which the path difference in the medium does not exceed the coherence length of radiation. The presence of such photon packets is explained by the fact that the sizes of scatterers and the distance between them are comparable with the coherence length. The consideration of these effects can result in a decrease in the contrast of the internal boundaries against the increased background of the total signal due to the randomness of the path difference of photon packets propagating in a strongly scattering paper sample. However, because of the random character of the paper structure, the distinct layer boundaries are absent in paper, resulting in a weak manifestation of these effects in real OCT images of paper samples [8].

To improve the whiteness and strength of paper, various fillers are used in modern paper production. We assume in simulations that filler particles have a spherical shape and their radii are varied from 0.1 to 1 μm. The scattering coefficient in a layer containing filler particles was set equal to 100 mm^{-1} assuming that the concentration of the filler is rather high, and the probability of photon scattering by a filler particle in the layer is rather high. We consider samples with a porosity of 44 %, assuming that filler particles are contained only in air layers.

Figure 5 presents the envelopes of the OCT signals from samples containing particles of different sizes. One can see

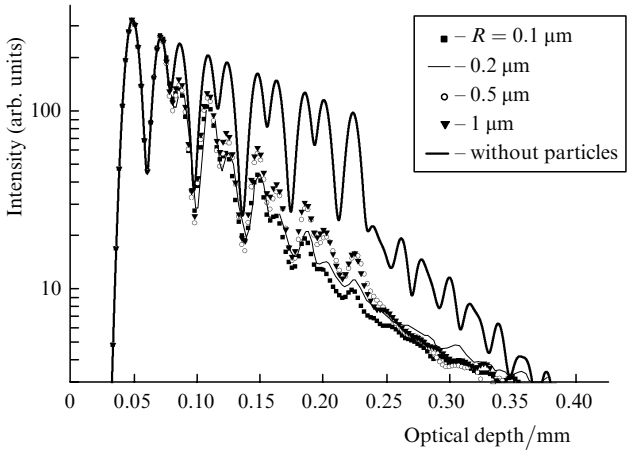

Figure 5. Envelopes of the model OCT signals from a paper sample with planar layers containing filler particles of different radii.

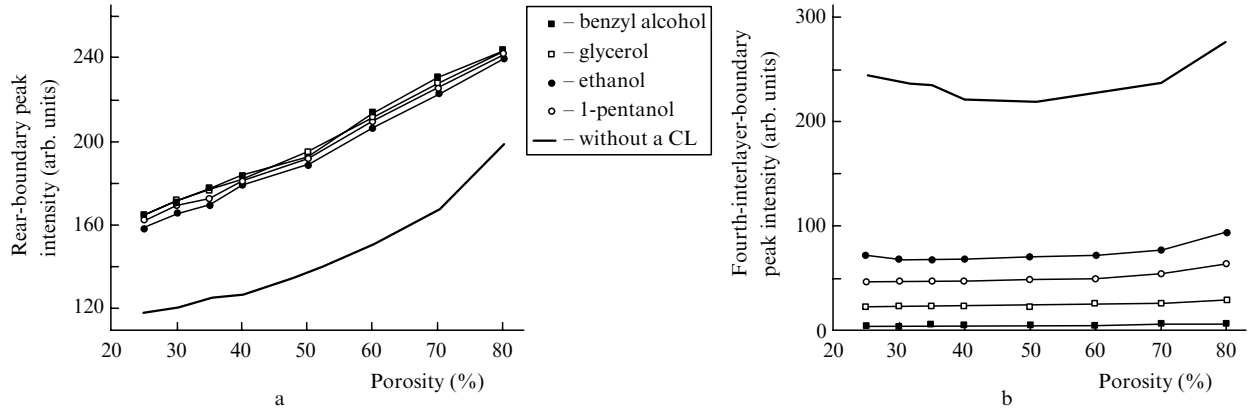

Figure 4. Dependences of the intensity of rear-boundary (a) and fourth-interlayer-boundary (b) peaks on the paper porosity obtained for different CLs.

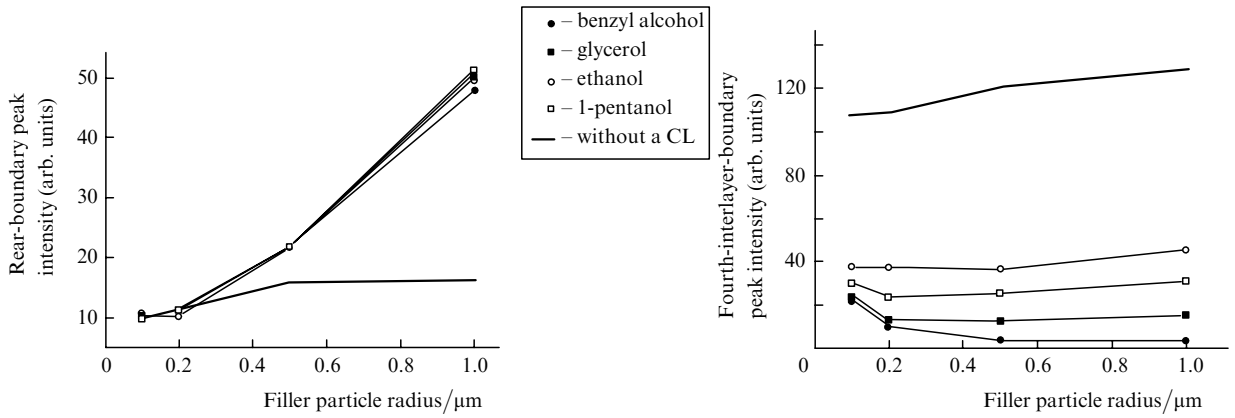

Figure 6. Dependences of the intensity of rear-boundary and fourth-interlayer-boundary peaks on the radius of filler particles obtained for different CLs.

that the filler reduces the intensities of the peaks corresponding to layer boundaries due to additional scattering. The smaller are the particles, the more isotropic is scattering from them. Multiple scattering also contributes to the signal, resulting in the appearance of a signal after the peak from the rear boundary of the layer. Distinct peaks in this part of the signal suggest that the signal is produced by photons multiply scattered from the boundaries of layers, whereas the absence of such peaks means that the signal is produced by photons scattered by the particles. One can see from the results obtained that the contrast of the OCT image of the rear boundary of the sample increases with increasing the radius of the filler particles. This is explained by the fact that the anisotropy of scattering by the particles increases and the medium becomes more transparent.

Figure 6 presents the dependences of the peak intensities in the model OCT signal on the filler particle radius. Although the peak intensity can decrease with increasing the particle radius due to the reduction of the contribution from multiple scattering, the best localisation of layer boundaries is achieved in the case of particles with large radii.

4.2 Paper samples with nonplanar layers

Because real layers from which paper consists are far from being plane–parallel, the model considered above is rather rough and can only qualitatively estimate the effect of a CL on the OCT imaging of paper. One can see from Fig. 1 that paper consists of fibre layers with nonplanar boundaries. To make our model more real and to study the effect of the boundary curvature, we simulated the two-dimensional images of paper samples for different shapes of layer boundaries. To obtain the analytic description, we considered layers with boundaries of the sinusoidal shape. First we simulated the OCT signals from samples for boundaries with a variable spatial frequency in order to estimate the influence of the spatial frequency on clearing. The surface shape was described by the expression

$$z(x) = a \sin\left(2\pi v x^2 + \frac{4\pi m}{10}\right), \qquad (3)$$

where $a = 2$ μm is the amplitude; $v = 6$ mm^{-1} is the spatial modulation frequency of the interlayer boundary; and $m = 1 - 8$ is the number of the interlayer boundary. The cross section of the simulated paper sample is shown in Fig. 7a. Figure 8 shows the model scans of paper samples with such geometry with and without the use of CLs. Each image consists of 100 successive A scans performed with the 10-μm intervals in the transverse direction. One can see from Fig. 8 that, as the spatial modulation frequency is increased, the contrast of the OCT image of the rear boundary of the sample without the use of a CL decreases. This occurs because in the case of a low spatial modulation frequency, photons are reflected almost strictly backward, contributing to small-angle scattering. As the spatial modulation frequency of the boundary is increased, the amplitude being the same, photons begin to reflect not strictly backward, especially from the sites that are not perpendicular to the initial direction of their propagation, and contribute to multiple scattering or do not contribute to the OCT signal at all, which deteriorates the contrast of the OCT image of the rear boundary of the sample. However, the sites that are perpendicular to the initial propagation direction of photons reflect them strictly backward. These sites in Fig. 8 correspond to intervals with the high radiation intensity against the weak-signal background. The visualisation of the rest of the elements of the boundary can be improved by increasing the numerical aperture of a detector.

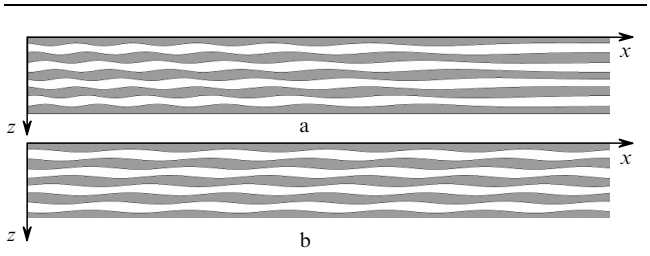

Figure 7. Cross sections of simulated paper samples with the variable (a) and constant (b) spatial modulation frequencies of layer boundaries. The size of each image is 1.00 mm along the x axis and 0.10 mm along the z axis.

The model images presented in Fig. 8 show that the use of CLs considerably improves the contrast of the OCT image of the rear boundary of a paper sample, although the quality of visualisation of its internal structure (interlayer boundaries) decreases. This effect is especially noticeable in regions with a high spatial frequency of interlayer boundaries. We estimated numerically the clearing effect for paper

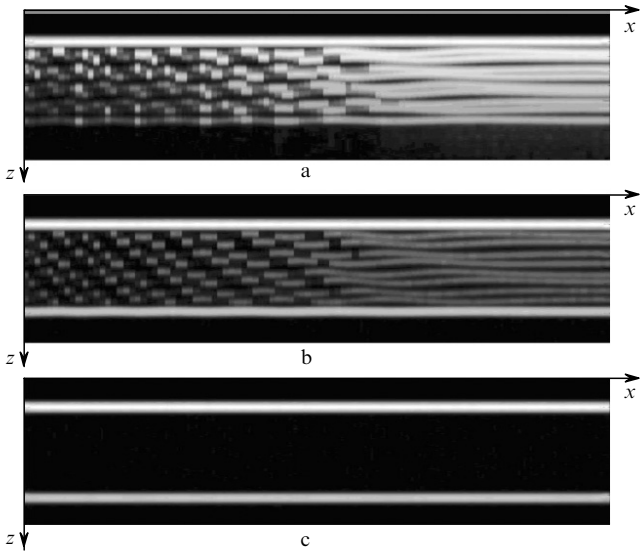

Figure 8. Model OCT images of paper samples (Fig. 7a) obtained without a CL (a) and with ethanol (b) and benzyl alcohol (c). The size of the scan region is 1.00 mm along the x axis and 0.25 mm along the z axis.

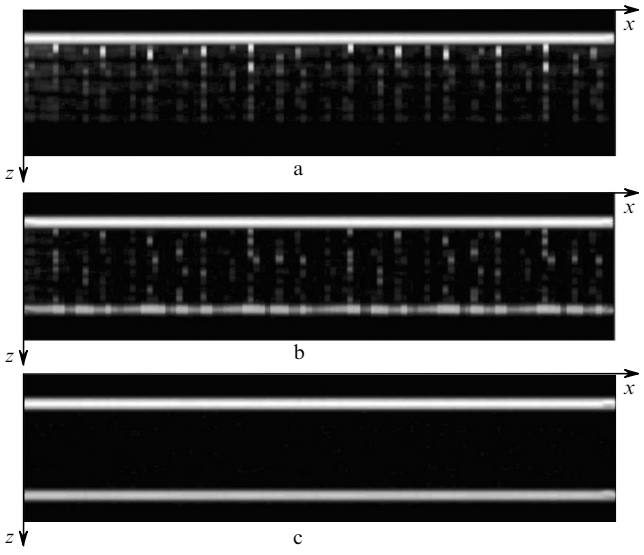

Figure 9. Model OCT images of paper samples (Fig. 7b) obtained without a CL (a) and with ethanol (b) and benzyl alcohol (c). The size of the scan region is 1.00 mm along the x axis and 0.25 mm along the z axis.

samples with $v = 6$ mm^{-1}. The surface of these samples can be described by the expression

$$z(x) = a\sin\left(2\pi v x + \frac{4\pi m}{10}\right). \quad (4)$$

To take into account microdefects of fibres in the model, we added a small random component to (4). As a result, the expression for boundaries took the form

$$z(x) = a\sin\left(2\pi v x + \frac{4\pi m}{10}\right) + \frac{a}{5}\sin(2\pi v x + \text{random}), \quad (5)$$

where $m = 1 - 8$ is the number of an interlayer boundary and 'random' is a random value uniformly distributed in the interval $[0, 2\pi]$. The cross section of such a paper sample is shown in Fig. 7b. The model OCT images of this sample are shown in Fig. 9. One can see that in the absence of a CL, the contrast of the OCT image of the rear boundary is very weak (Fig. 9a), however, as in the previous case, it increases when a CL is used (Figs 9b, c).

To estimate quantitatively the influence of CLs on the OCT image contrast of the rear boundary of a sample, we averaged the A scan over 100 realisations in each model image and compared the intensities of the rear-boundary peaks in the averaged scan. We considered two models of samples with interlayer boundaries described by expressions (4) and (5).

The results of the comparison are presented in Fig. 10. One can see that for the model of a paper sample with interlayer boundaries described by expression (4), the effect of all CLs is virtually the same: the contrast of the OCT image of the rear boundary increases twice compared to that of a dry sample. Note, however, that this model is idealised, while the model represented by expression (5) better describes the real structure of paper. It follows from the results obtained that the contrast of the OCT image of the rear boundary of a sample without a CL with boundaries described by expression (4) is seven times lower than that with boundaries described by expression (5), which is explained by strong scattering from microscopic irregularities caused by the random component and the corresponding change in the propagation direction of a photon.

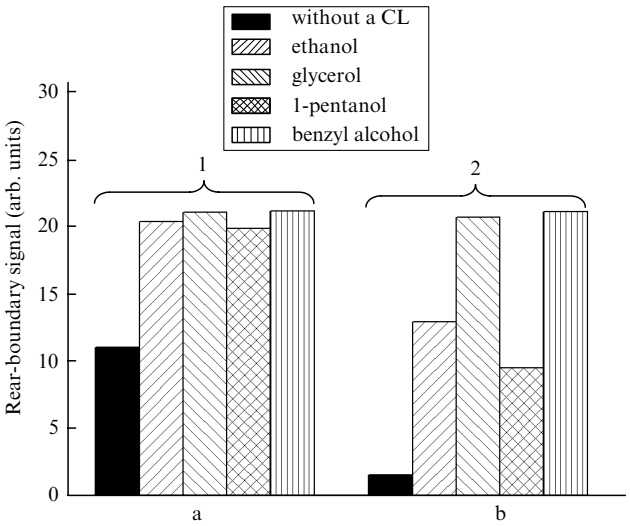

Figure 10. Contrast of the OCT image of the rear boundary of a sample without (a) and with (b) the use of CLs for the interlayer boundaries without (1) and with (2) a random component.

Figure 10 also demonstrates a strong dependence of the degree of paper clearing on the CL type in the case of boundaries with microscopic irregularities. All the CLs considered here provide a significant increase in the contrast of the OCT image of the rear boundary due to a decrease in the difference of refractive indices at the boundary and a weaker chaotisation of the propagation direction of photons. The best visualisation is provided by glycerol or benzyl alcohol, whose refractive indices are most close to the refractive index of paper fibres. The treatment of samples with these CLs enhanced the OCT image contrast of the rear boundary by an order of magnitude compared to that before the treatment. Thus, glycerol and benzyl alcohol can be efficiently used for the visualisation of the rear boundary of paper samples, which is important for precision measure-

ments of their thickness. The results obtained in the paper are in good agreement with experiments performed in [8], which have shown that benzyl alcohol is the best CL for OCT studies of paper.

5. Conclusions

Analysis of the results obtained in the paper has shown that all the CLs studied above improve the visualisation of the rear boundary of paper samples, which is important for precision OCT measurements of the paper thickness, in particular, for the paper quality control. The best visualisation of the rear boundary of a paper sample is achieved by using CLs with the refractive indices close to that of wood fibres [glycerol ($n = 1.47$) and benzyl alcohol ($n = 1.54$)]. Note, however, that the image contrast of the internal structure of the sample decreases in this case. Analysis of the results obtained for the model of planar layers has shown that the OCT image contrast of the rear boundary increases with increasing the paper porosity. The presence of filler particles reduces the OCT image contrast of layer boundaries because scattering by particles is more isotropic than by paper fibres. The larger is the particle size, the higher is anisotropy and, hence, the better is the rear-boundary visualisation.

The study of nonplanar interlayer boundaries has shown that the contrast of their OCT image in the absence of CLs is substantially lower than that in the case of planar boundaries. We have found that the best CLs for all the models considered are benzyl alcohol and glycerol, whose refractive indices are most close to the refractive index of wood fibres. The results obtained in the paper are in good agreement with experimental data [8].

Acknowledgements. This work was partially supported by the Leading Scientific School of Russia (Grant No. 2071.2003.4), GETA Graduate School, and Infotech Oulu Graduate School.

References

1. Myllylä R., Alarousu E., Fabritius T., et al. *PALS'03. Book of Abstracts* (Saratov, 2003) p. 26.
2. Huang D., Swanson E.A., Lin C.P., et al. *Science*, **254**, 1178 (1991).
3. Tuchin V.V. *J. Phys. D: Appl. Phys.*, **38**, 2497 (2005).
4. Kirillin M., Priezzhev A.V., Alarousu E., et al. *PALS'03. Book of Abstracts* (Saratov, 2003) p. 39.
5. Meglinskiĭ I.V., Bashkatov A.N., Genina E.A., Churmakov D.Yu., Tuchin V.B. *Kvantovaya Elektron.*, **32**, 875 (2002) [*Quantum Electron.*, **32**, 875 (2002)].
6. He Y., Wang R.K. *J. Biomed. Opt.*, **9**, 200 (2004).
7. Tuchin V.V. *J. Biomed. Opt.*, **4**, 106 (1999).
8. Fabritius T., Alarousu E., Prykäri T., Hast J., Myllylä R. *Kvantovaya Elektron.*, **36**, 181 (2006) [*Quantum Electron.*, **36**, 181 (2006)].
9. Yao G., Wang L.V. *Phys. Med. Biol.*, **44**, 2307 (1999).
10. Wang R.K. *Phys. Med. Biol.*, **47**, 2281 (2002).
11. Schmitt J.M., Knuttel A., Yadlowsky M., et al. *Phys. Med. Biol.*, **39**, 1705 (1994).
12. Lindimo T., Smithies D., Chen Z., et al. *Phys. Med. Biol.*, **43**, 3045 (1998).
13. Kirillin M., Priezzhev A.V., Kinnunen M., et al. *Proc. SPIE Int. Soc. Opt. Eng.*, **5325**, 164 (2004).
14. Meglinski I.V., Matcher S.J. *Physiol. Meas.*, **23**, 741 (2002).
15. Borch J., et al. *Handbook of Physical Testing of Paper* (New York: Marcel Dekker, 2002) Vol. 2.
16. Green K., Lamberg L., Lumme K. *Appl. Opt.*, **39**, 4669 (2000).
17. Carlsson J., Hellentin P., et al. *Appl. Opt.*, **34**, 1528 (1995)